Am J Transl Res 2017;9(7):3399-3410
www.ajtr.org /ISSN:1943-8141/AJTR0052668

Original Article

Anti-tumor efficacy evaluation of a novel monoclonal antibody targeting neutral amino acid transporter ASCT2 using patient-derived xenograft mouse models of gastric cancer

Noriyuki Kasai[1*], Aya Sasakawa[2*], Kenta Hosomi[2], Tze Wei Poh[1], Bernadette Lynn Chua[1], Wei Peng Yong[3], Jimmy So[4], Shing Leng Chan[5], Richie Soong[5], Koji Kono[6], Toshihiko Ishii[2], Kazuya Yamano[1]

[1]Singapore Translational Research Laboratory, Kyowa Hakko Kirin (Singapore) Pte. Ltd., 11, Biopolis Way, 138667, #05-08 Helios, Singapore; [2]R&D Division, Kyowa Hakko Kirin Co. Ltd., Shizuoka, Japan; [3]Department of Haematology-Oncology, National University Cancer Institute, Singapore; [4]Department of Surgery, National University Health System, Singapore, Singapore; [5]Cancer Science Institute of Singapore, National University of Singapore, Singapore; [6]Department of Surgery, National University of Singapore, Singapore. [*]Equal contributors.

Received March 11, 2017; Accepted June 1, 2017; Epub July 15, 2017; Published July 30, 2017

Abstract: ASC amino acid transporter 2 (ASCT2), also known as solute linked carrier family 1 member A5 (SLC1A5) is a Na+-dependent glutamine/neutral amino acid transporter. ASCT2 acts as a high-affinity transporter of L-glutamine (Gln) and has been reported to be up-regulated in a variety of cancerous tissues including stomach, liver, and kidney. In this study, we evaluated anti-tumor efficacy of a novel anti-ASCT2 humanized monoclonal antibody, KM8094, which has a neutralizing activity against glutamine uptake, as a therapeutic antibody against gastric cancer and explored clinical predictive biomarker candidates by utilizing patient-derived xenograft (PDX) mouse models. Anti-tumor efficacy studies revealed that some of the PDX models used were responsive to KM8094 and the others were not. Interestingly, we observed a correlation between anti-tumor efficacy and low antigen expression as well as low basal levels of glutamine uptake, suggesting ASCT2 expression level could be a potential predictive biomarker for KM8094. We then further explored predictive biomarker candidates by multi-omics analysis on gastric cancer PDX mouse models. As a result, a few potential candidates such as TFF2, MUC13, and ANG were selected by gene expression and DNA methylation array analyses. In addition, metabolomics analysis revealed clear differences in intracellular energy status and redox status between responsive and non-responsive PDX models.

Keywords: ASCT2, antibody, patient-derived xenograft model, gastric cancer, biomarker

Introduction

Gastric cancer is a leading cause of global cancer mortality with an overall 5-year survival rate of approximately 20% [1, 2]. Gastric cancers are particularly prevalent in many Asian countries [3]. Most gastric cancer patients are diagnosed at advanced disease stages and thus treatment options are often limited. Meanwhile, in addition to standard cytotoxic regimens, targeted therapies, which are small molecules or antibodies designed to target specific oncogenic signaling pathways, have recently emerged as a promising therapeutic strategy.

ASC amino acid transporter 2 (ASCT2), also known as solute linked carrier family 1 member A5 (SLC1A5) is a Na+-dependent glutamine/neutral amino acid transporter. ASCT2 acts as a high-affinity transporter of L-glutamine (Gln) particularly in rapidly growing epithelial and tumor cells in culture [4] and has been reported to be up-regulated in a variety of cancerous tissues including stomach, liver, and kidney [5]. As compared to normal cells, cancer cells display enhanced and altered channeling of amino acids into select metabolic pathways, often in concert with the aerobic glycolysis of tumors [6, 7]. Furthermore, several studies revealed a new role of ASCT2 that is independent from glutamine metabolism and necessary for activating critical survival and cellular growth signaling cascades in cancer, which includes mTOR and ERK pathways [8, 9]. It is to be noted that block-

ade of ASCT2-related Gln uptake in lung cancer cells increased release of intracellular ROS, and targeting ASCT2 caused G1 arrest by inhibiting mTOR signaling [10]. Moreover, shRNA knockdown of ASCT2 in prostate cancer cell line xenograft models significantly inhibited tumor growth and metastasis *in vivo* [11]. Taking these reports into account, ASCT2 is a potential cancer therapeutic target.

Recently, a report on an anti-ASCT2 monoclonal antibody developed by Kyowa Hakko Kirin (Tokyo, Japan), which has a neutralizing activity against glutamine uptake, has been published [12]. In this study, we evaluated anti-tumor efficacy of its humanized derivative antibody (IgG1), KM8094, as a therapeutic antibody against gastric cancer and explored clinical biomarker candidates by utilizing patient-derived xenograft (PDX) mouse models. Utility of PDX models for drug discovery, drug efficacy evaluation and biomarker finding is increasingly being recognized, with their opportunities and limitations in cancer drug development having been covered in multiple reviews [13-15]. This report demonstrates the therapeutic potential of our novel anti-ASCT2 monoclonal antibody and also suggests some clinical biomarkers candidates that could be used to predict its efficacy.

Materials and methods

Materials

A defucosylated humanized anti-human ASCT2 monoclonal antibody KM8094 (IgG1) was produced by Kyowa Hakko Kirin (Tokyo, Japan). KM8094 is a humanized derivative antibody of KM4008, a mouse monoclonal antibody which specifically binds to the natural configuration of an extracellular domain of ASCT2 [12]. A negative control monoclonal antibody, KM8047 (defucosylated human anti-dinitrophenol antibody IgG1), was also obtained from Kyowa Hakko Kirin. Other chemicals and reagents were of the highest grade and purchased from local commercial sources.

Histologic analysis and immunohistochemistry (IHC) on tumor specimens of gastric cancer patient-derived xenograft mouse models

We conducted histologic analysis and IHC using tumor specimens of gastric cancer patient-derived xenograft mouse models; GC117, GC119, GC127, GC84, and GC113. The tumor tissues from which the five PDX models were generated were provided by Dr. Chan Shing Leng (NUS, Singapore). Clinical data of patients used for establishment of gastric cancer PDX models are described in Supplementary Table 1.

Haematoxylin and eosin (H&E) staining on paraffin sections (4 μm) was carried out by Advanced Molecular Pathology Laboratory (AMPL, A*STAR, Singapore). H&E images for primary tumor sections from gastric cancer patients were given by Dr. Chan Shing Leng (NUS, Singapore). ASCT2 expression on tissue sections was determined by IHC.

Frozen sections (6 μm) were fixed in 4% PFA, after which, endogenous peroxidase was quenched, followed by avidin/biotin blocking. The sections were then exposed to 10 μg/ml KM8094 biotin conjugate for 1 h at room temperature. Anti-biotin antibody (VECTASTAIN Kit, Vector Laboratory) was applied for 30 min at room temperature and the color was then developed using DAB substrate chromogen prepared from DAB tablet (Wako Pure Chemical Industries) for 4 min at room temperature.

Dissociation of tumor tissue

Tumor tissues were dissociated in 9 ml DMEM-F12 (Life Tech) digestion media (2% BSA, 5 mg collagenase, 1 μg/ml hydrocortisone, 1 ampoule of hyaluronidase (all from Sigma), 5 μg/ml insulin and 1% antibiotic-antimycotic (all from Life Tech) with shaking for 2 h, at 37°C. Dead cells were removed using the dead cell removal kit (Miltenyi Biotec). Live cells from dissociated tumor tissues were subsequently used for analysis by flow cytometry as well as for the glutamine uptake assay.

Analysis of ASCT2 levels in gastric cancer patient-derived xenograft mouse models by flow cytometry

ASCT2 levels on dissociated tumor cells from GC117, GC119, GC127, GC84, and GC113 were evaluated by flow cytometry using 20 μg/ml KM8094 or KM8047 (control article) and 20 μg/ml PE-conjugated goat anti-human IgG monoclonal antibody (Southern Biotech) as a secondary antibody.

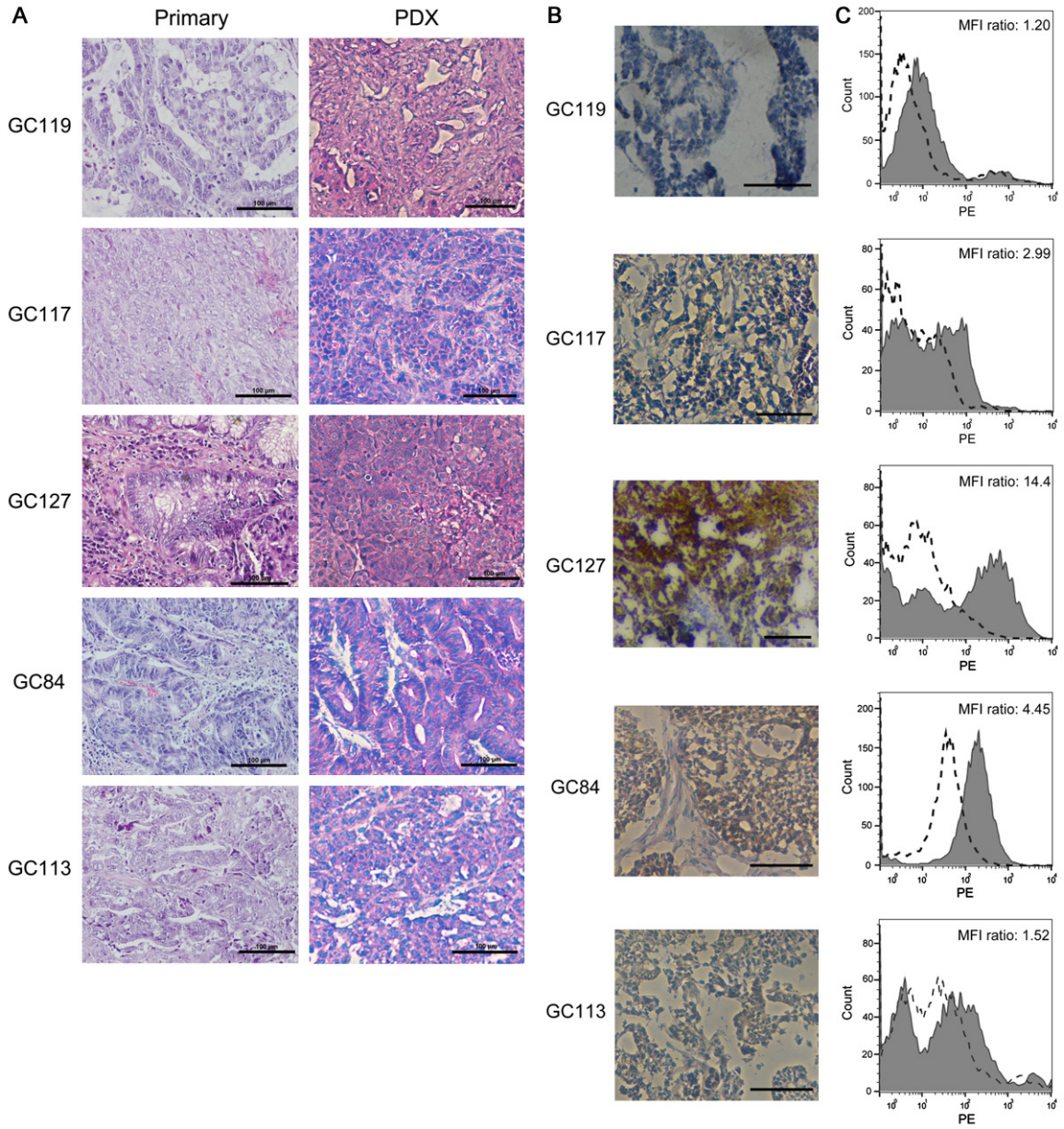

Figure 1. Histologic and antigen expression analysis on tumor specimens of gastric cancer patient-derived xenograft mouse models. A. Histologic images of PDX sections were obtained by staining paraffin sections with hematoxylin-eosin. B. Immunohistochemical images of ASCT2 were obtained by staining frozen sections using biotinylated KM8094 and its secondary antibody. Scale bar represents 100 μm. C. Binding activity of KM8094 to tumor cells were analyzed by flow cytometry. Cells were incubated either with KM8047 (control antibody, broken line histogram) or KM8094 (grayed histograms), and stained with PE-conjugated goat anti-human IgG monoclonal antibody as the secondary antibody. The MFI ratio was calculated according to the following formula: MFI ratio = (S)/(C) where S is the MFI of cells stained by KM8094, C is the MFI of cells stained by KM8047 (MFI: mean fluorescent intensity).

The effect of KM8094 on glutamine uptake in gastric cancer patient-derived xenograft mouse models

Dissociated tumor cells were plated at 10^5 cells/well in a 96-well U bottomed plate. KM-8094 or KM8047 was added at 30 μg/ml to the cells for 15 min at 37°C, following which, ^{3}H-glutamine (Perkin Elmer) was then added to the cells for uptake at 37°C for 15 min. After the excess ^{3}H-glutamine was washed off, cells were lysed in NP-40 buffer (Invitrogen) and the amount of ^{3}H-glutamine taken up by the cells was read on a LumaPlate (PerkinElmer) by

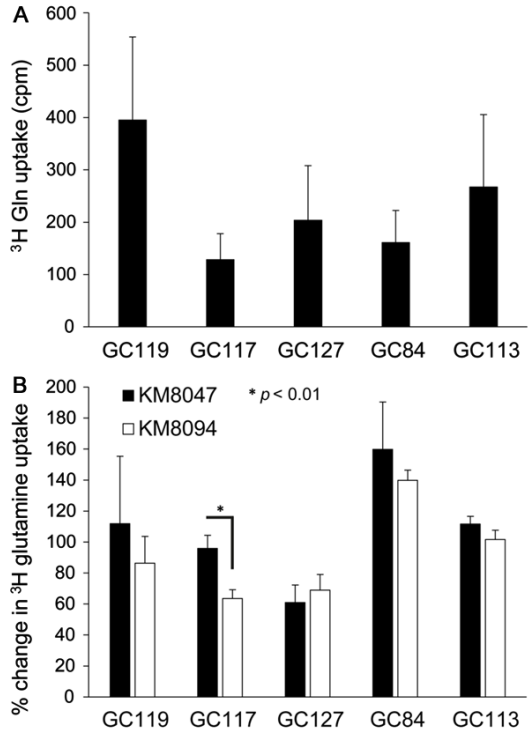

Figure 2. The effect of KM8094 on glutamine uptake in gastric cancer patient-derived xenograft mouse models. A. Basal level of ^{3}H glutamine uptake in PDX lines. The graph represents the average values (in count per minute) obtained from 2-5 individual experiments for each PDX line. B. Inhibition of ^{3}H glutamine uptake in PDX lines by 30 μg/ml KM8047 or KM8094. The results are shown on the graph as a percentage change from the basal level (no antibody treatment) of ^{3}H glutamine uptake in each PDX line. The graph represents the average percentage change obtained from 2-5 individual experiments for each PDX line. Bars represent standard deviation.

Microbeta2 (PerkinElmer). Statistical significance was analyzed using student's t test in Microsoft Excel.

Anti-tumor efficacy of KM8094 in gastric cancer patient-derived xenograft mouse models

Animal experiments: All animal experiments were conducted with the approval of Institutional Animal Care and Use Committee (IACUC) in the National University of Singapore (NUS) and Biological Resource Centre (BRC) in A*Star (Singapore). C.B-Igh-1^b/IcrTac-Prkdc^{scid} (SCID) male mice were purchased from InVivos (Singapore). For each PDX model, each tumor tissue passaged via mice was inoculated subcutaneously with a trocar into 65-80 SCID mice. Passage numbers at dosing for GC117, GC119, GC127, GC84, and GC113 were 8, 8, 7, 13, and 11, respectively. After the tumors grew to about 200 mm^3, 20 mice were selected and divided into two groups (10 mice each except for GC119:1 mouse missing in the vehicle control group). The mice received bolus injection of PBS (vehicle, Invitrogen) or KM8094 (10 mg/kg) from tail vein once weekly for 2 weeks for GC119 or 3 weeks for the other PDX lines. Vehicle and the antibody solutions were administered at a volume of 5 ml/kg body weight. Body weight and tumor volume of the mice were measured once or twice a week.

Statistical methods for analysis of raw data for the animal experiments: Tumor volume was calculated using Microsoft® Excel 2007 as follows: tumor volume = DL × DS × DS × 1/2 (DL, long diameter; DS, short diameter). Statistical analysis was performed using the SAS software program (Release 9.2, SAS Institute), in which tumor volume on the last day was used as a parameter. Significant differences between the KM8094-treated group and the vehicle-treated group were analyzed by Student's t-test or Aspin-Welch t-test. In these tests, P<0.05 was considered significant.

Identification for predictive biomarker candidates by multi-omics analysis on gastric cancer patient-derived xenograft mouse models

Gene expression array analysis: Total RNA was extracted using RNeasy Mini Kit (Qiagen) from tumor tissues of GC117, GC119, GC84, and GC127. The gene expression array analysis was conducted in triplicate using tumor tissues from three individual mice for each PDX model. Gene expression profiling was performed using Illumina Human HT-12 v4 Bead-Chips. For each sample, 250 ng of total RNA was labeled using an Illumina TotalPrep-96 RNA Amplification Kit (Ambion) according to the manufacturer's instructions. The arrays were scanned using HiScan Array Scanner (Illumina). The output gene list table was ordered by fold difference of gene expression of responders (GC117 and GC119) against non-responders (GC84 and GC127). We defined responders and non-responders based on the results of anti-tumor efficacy tests (**Figure 2**). We used 0.05 as a threshold for both a paired t-test p-value and a false discovery rate (FDR).

DNA methylation array analysis: Genomic DNA was extracted using QIAmp DNA Mini Kit (Qiagen) from tumor tissues of GC117, GC119,

GC84, and GC127. The DNA methylation analysis was conducted in triplicate using tumor tissues from three individual mice for each PDX model. Array-based specific DNA methylation analysis was performed with the Infinium Human Methylation 450K bead chip technology (Illumina). The arrays were scanned using HiScan Array Scanner (Illumina). The output gene list table was ordered by fold difference of DNA methylation of responders (GC117 and GC119) against non-responders (GC84 and GC127). We used 0.05 as a threshold for FDR.

Metabolomics analysis: Metabolome measurements were carried out through a facility service at Human Metabolome Technologies (HMT, Tsuruoka, Japan). Frozen tissues taken from GC117, GC119, GC84, and GC127 were plunged into 50% acetonitrile/Milli-Q water containing internal standards (HMT) at 0°C in order to inactivate enzymes. The tissues were homogenized at 1,500 rpm for 120 s using a tissue homogenizer (Microsmash MS100R, Tomy Digital Biology) and then the homogenate was centrifuged at 2,300 × g and 4°C for 5 min. Subsequently, the upper aqueous layer was centrifugally filtered through a Millipore 5-kDa cutoff filter at 9,100 × g and 4°C for 120 min to remove proteins. The filtrate was centrifugally concentrated and re-suspended in 50 μl of Milli-Q water for CE-MS analysis. The metabolomics analysis was conducted in triplicate using tumor tissues from three individual mice for each PDX model. The following parameters were calculated by the formula below.

$$\text{Adenylated Energy Charge} = \frac{[\text{ATP}] + 0.5 \times [\text{ADP}]}{[\text{ATP}] + [\text{ADP}] + [\text{AMP}]}$$

Total Adenylate=[ATP]+[ADP]+[AMP]

$$\text{Guanylate Energy Charge} = \frac{[\text{GTP}] + 0.5 \times [\text{GDP}]}{[\text{GTP}] + [\text{GDP}] + [\text{GMP}]}$$

Total Guanylate=[GTP]+[GDP]+[GMP]

Results

Analysis of ASCT2 levels and function in gastric cancer PDX lines

Histologic analysis revealed that the gastric cancer PDX lines used in our studies were similar to their primary tumors (**Figure 1A**). Analysis of ASCT2 levels in PDX samples by immunohistochemistry (**Figure 1B**) and flow cytometry (**Figure 1C**) showed that there were varying levels of ASCT2 expression among the five PDX lines. The highest level of ASCT2 expression was seen in GC127, using immunohistochemistry (**Figure 1B**) and flow cytometry (**Figure 1C**). Given the varying levels of ASCT2 expression among the five PDX lines, we sought to determine if glutamine uptake in these PDX lines would also vary in a similar manner. Intriguingly, GC119 showed the highest uptake of ^{3}H glutamine uptake while GC117 showed the lowest (**Figure 2A**).

In vitro and in vivo efficacy of KM8094 in gastric cancer PDX lines

We proceeded to analyze the efficacy of KM8094 *in vitro* via the ^{3}H-glutamine uptake assay and *in vivo* by determining the anti-tumor efficacy of KM8094 in gastric cancer PDX lines. KM8094 significantly inhibited ($P< 0.01$) ^{3}H-glutamine uptake in GC117 at 30 mg/ml as compared to the control antibody, KM8047 (**Figure 2B**). With the exception of GC127, we observed trends of lower ^{3}H-glutamine uptake in all other PDX lines as compared to the control antibody, KM8047, however these differences did not prove to be statistically significant.

The *in vivo* anti-tumor efficacy of KM8094 in the five PDX lines is shown in **Figure 3**. Statistically significant differences in the mean tumor volumes between the KM8094-treated group and the vehicle control-treated group were observed for GC119 and GC117. The mean tumor volumes in the KM8094-treated group were consistently lower than those in the control-treated group in GC113, although the differences between the two groups were not statistically significant.

Identification of predictive biomarker candidates by multi-omics analysis on gastric cancer PDX lines

Given that not all PDX lines responded equally to KM8094 *in vivo*, we conducted multi-omics (gene expression, DNA methylation, and metabolomics) exploration for biomarker candidates that could be used to predict PDX models response to KM8094 prior to treatment.

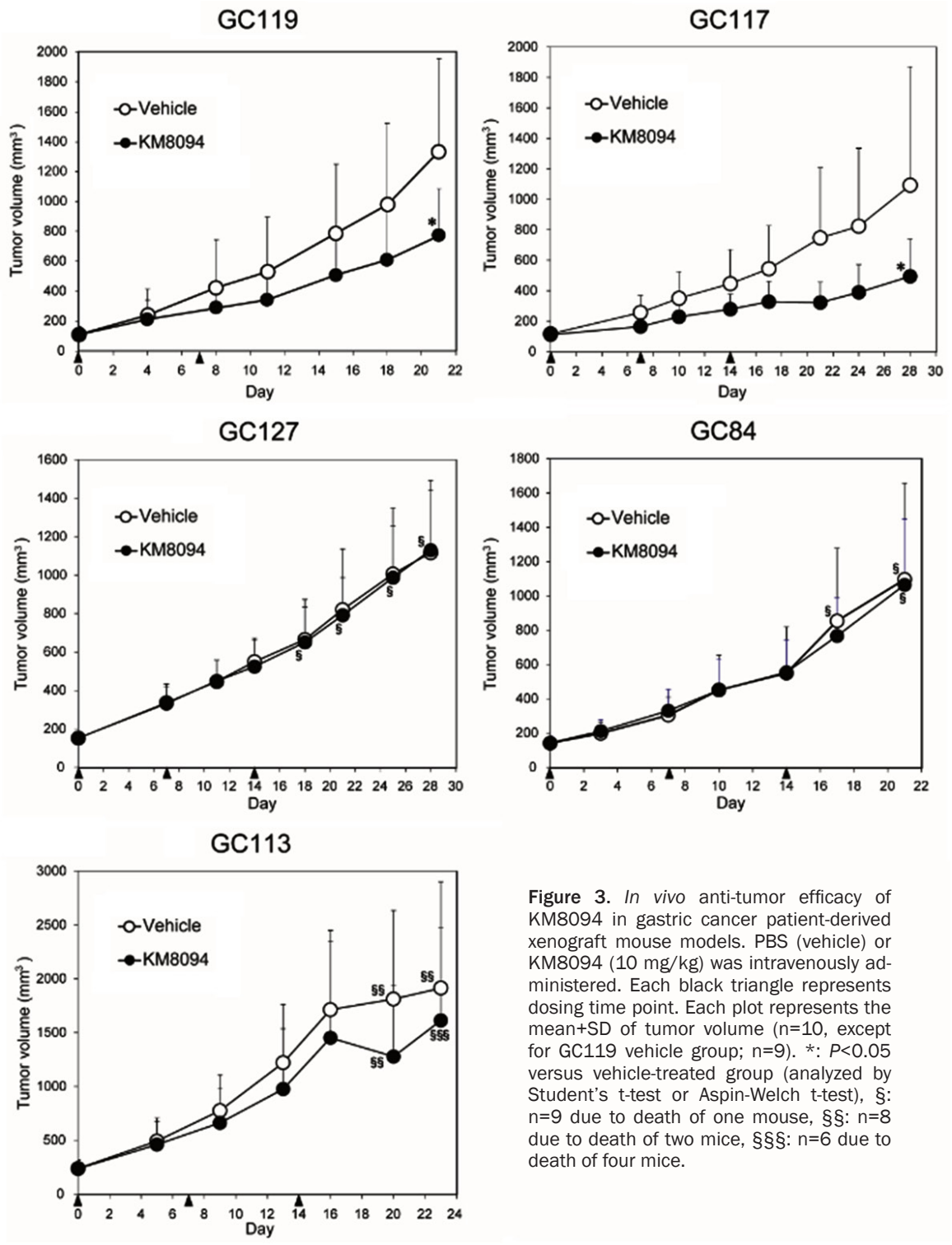

Figure 3. *In vivo* anti-tumor efficacy of KM8094 in gastric cancer patient-derived xenograft mouse models. PBS (vehicle) or KM8094 (10 mg/kg) was intravenously administered. Each black triangle represents dosing time point. Each plot represents the mean+SD of tumor volume (n=10, except for GC119 vehicle group; n=9). *: $P<0.05$ versus vehicle-treated group (analyzed by Student's t-test or Aspin-Welch t-test), §: n=9 due to death of one mouse, §§: n=8 due to death of two mice, §§§: n=6 due to death of four mice.

Gene expression and DNA methylation array analyses: Based on their response to KM8094 *in vivo* (**Figure 3**), we conducted gene expression and DNA methylation array analyses on four untreated PDX lines that have been grouped into responders (GC117 and GC119) and non-responders (GC84 and GC127). The output gene list was ordered by differential gene expression of responders against non-responders, according to conditions described in Materials and Methods. There were a total of 11 genes that were upregulated by more

A

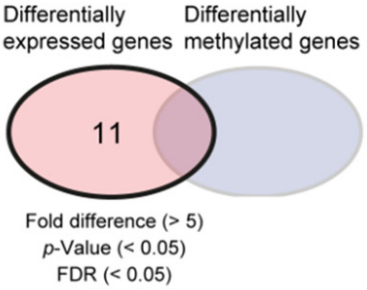

Gene	Fold difference
TFF2	81.32
CMBL	20.87
PI3	17.76
MUC13	10.12
RARRES3	9.20
SMIM24	8.01
ANG	7.17
TM4SF20	6.62
IFI27	6.53
RAC2	5.88
ECHDC3	5.19

B

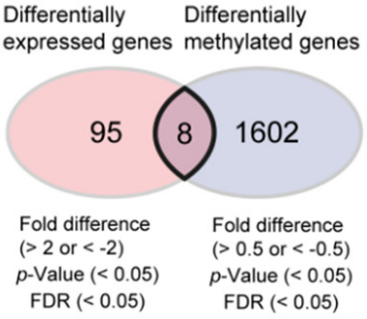

	Gene expression	Methylation	
Gene	Fold difference	Distance to TSS	Fold difference
ANG	7.18	4135	3.06
CMBL	20.87	1222	-3.29
CRISPLD2	2.12	-421	4.07
HIST1H1C	4.43	2148	-2.97
KCNS1	2.31	-156	-22.88
LRG1	3.09	34	-37.21
PLCL2	2.67	-744	-20.79
RNASE4	3.29	4099	3.06

Figure 4. Candidate lists for predictive biomarkers identified by multi-omics analysis on gastric cancer patient-derived xenograft mouse models. A. Predictive biomarker candidates identified by analyzing fold difference of gene expression data between responders (GC117 and GC119) and non-responders (GC84 and GC127). TFF2: trefoil factor 2, CMBL: carboxymethylenebutenolidase homolog (Pseudomonas), PI3: peptidase inhibitor 3, skin-derived, MUC13: mucin 13, cell surface associated, RARRES3: retinoic acid receptor responder (tazarotene induced) 3, SMIM24: small integral membrane protein 24, ANG: angiogenin, ribonuclease, RNase A family, 5, TM4SF20: transmembrane 4 L six family member 20, IFI27: interferon, alpha-inducible protein 27, RAC2: ras-related C3 botulinum toxin substrate 2, ECHDC3: enoyl CoA hydratase domain containing 3. B. List of genes selected by analyzing fold difference of gene expression and DNA methylation data between responders and non-responders. TSS represents transcription start site. CRISPLD2: cysteine-rich secretory protein LCCL domain containing 2, HIST1H1C: histone cluster 1, H1c, KCNS1: potassium voltage-gated channel, modifier subfamily S, member 1, LRG1: leucine-rich alpha-2-glycoprotein 1, PLCL2: phospholipase C-like 2, RNASE4: ribonuclease, RNase A family, 4.

than 5 fold in responders, as compared to non-responders (**Figure 4A**). The expression level of TFF2 (trefoil factor 2) in responders was the highest among these candidates and none of these candidates showed differential DNA methylation. On the other hand, there were no genes that were down-regulated in responders by more than 5 fold with significant *p*-value and FDR. However, it is to be noted that ASCT2 gene expression in responders was more than 5 times lower than that in non-responders although the FDR was higher than that described in Materials and Methods (*p*-value: 0.0021, FDR: 0.0709, fold difference: -5.597). Besides that, one hundred and three genes were found to be differentially expressed by more than 2 fold in responders, as compared to non-responders. Of which, 8 of these genes were found to have 0.5 fold differential DNA methylation and are listed in **Figure 4B**.

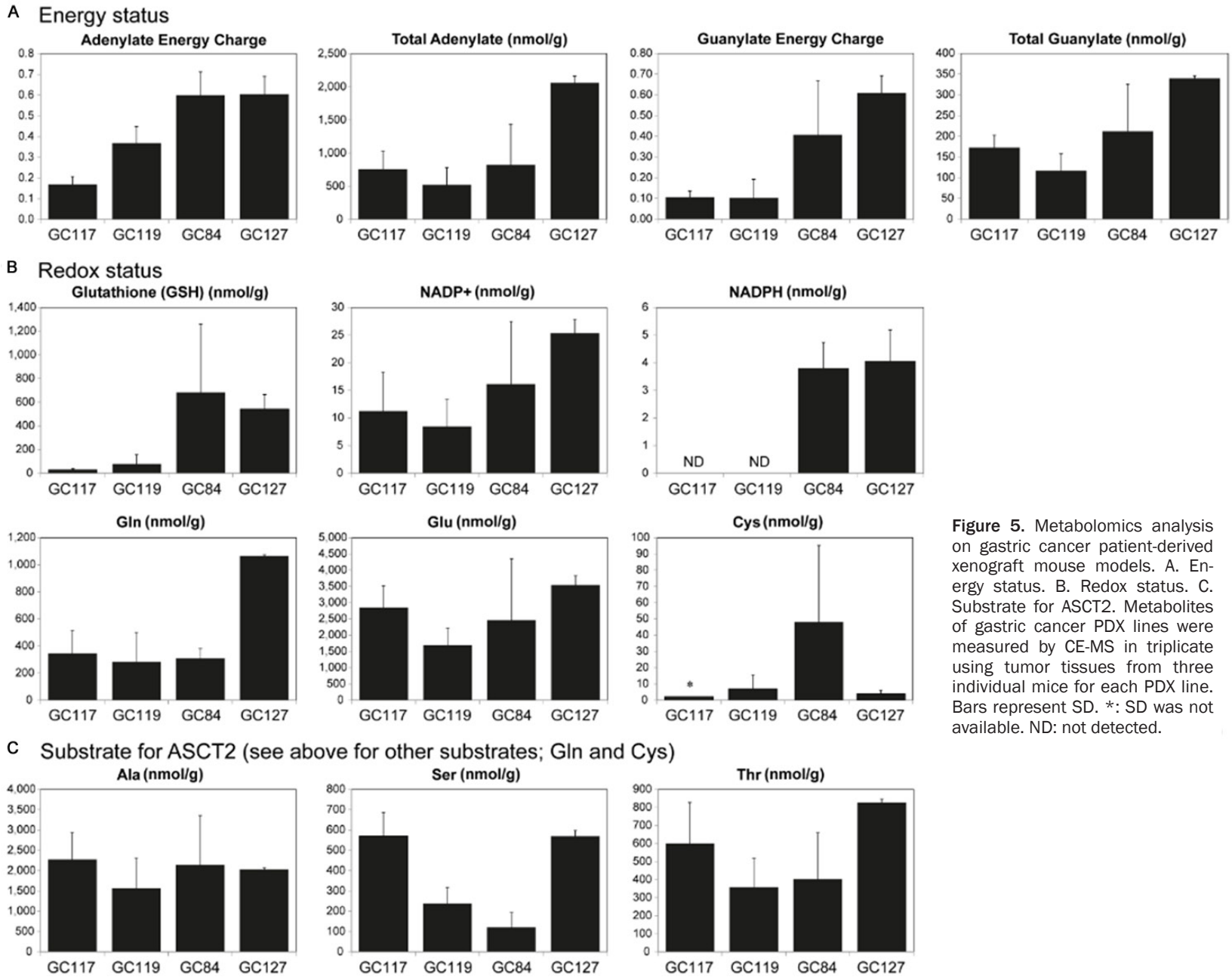

Figure 5. Metabolomics analysis on gastric cancer patient-derived xenograft mouse models. A. Energy status. B. Redox status. C. Substrate for ASCT2. Metabolites of gastric cancer PDX lines were measured by CE-MS in triplicate using tumor tissues from three individual mice for each PDX line. Bars represent SD. *: SD was not available. ND: not detected.

Metabolomics analysis: The differences in basal level uptake of glutamine in the PDX lines suggest inherent metabolic differences that might be responsible for the varying efficacy of KM8094 *in vitro* and *in vivo*. We measured a wide range of metabolites in tumors taken from GC117, GC119, GC84, and GC127, of which, the parameters, adenylate energy charge (AEC) and guanylate energy charge (GEC), representing intracellular energy status, were prominently higher in non-responders (**Figure 5A**). Furthermore, GSH and NADPH, which have reducing ability, were also higher in non-responders (**Figure 5B**). In addition, some of the substrates for ASCT2, Gln and Cys were clearly high in GC127 and GC84, respectively, which have been defined as a non-responder (**Figure 5C**).

Discussion

ASCT2, also known as SLC1A5, is a Na+-dependent glutamine/neutral amino acid transporter. ASCT2 acts as a high-affinity transporter of L-glutamine (Gln) and has been reported to be up-regulated in a variety of cancer types [5]. Recently, a novel anti-ASCT2 monoclonal antibody with a neutralizing activity against glutamine uptake has been reported [12]. In this translational study, we evaluated anti-tumor efficacy of its humanized derivative antibody (IgG1), KM8094 as a therapeutic antibody against gastric cancer and explored clinical predictive biomarker candidates by utilizing PDX mouse models.

Low expression levels of ASCT2 and low basal levels of glutamine uptake can contribute to the anti-tumor efficacy of KM8094

In our study, H&E sections showed that there were no major differences between PDX lines and the primary tumor from which each PDX line was generated (**Figure 1A**). All the PDX models used were intestinal type according to the Lauren classification [16] and the differentiation levels ranged from moderate to poor. There were varying levels of ASCT2 expression among the PDX lines based on the staining intensities in the IHC images (**Figure 1B**). Similarly, the ASCT2 expression levels analyzed by IHC were consistent with the results obtained by flow cytometry (**Figure 1C**).

GC119 and GC117 with low levels of ASCT2 were sensitive to anti-tumor effect of KM8094, as evidenced by statistically significant differences in the mean tumor volumes between the KM8094-treated group and the vehicle control-treated group (**Figure 3**). A similar trend was observed in GC113, which also expressed low levels of ASCT2. On the other hand, GC84 and GC127, which had higher antigen expression levels, were not susceptible to anti-tumor effect of KM8094. Overall, GC117 was the most sensitive to the treatment with KM8094 as demonstrated by statistically significant decreases in glutamine uptake ($P<0.01$) *in vitro* as well as the greatest reduction in tumor growth *in vivo*. Based on the results, it would appear the anti-tumor efficacy of KM8094 is inversely correlated with expression levels of ASCT2 as well as basal levels of glutamine uptake. GC117 had both low expression of ASCT2 and low basal levels of glutamine uptake, thus KM8094 showed most potent anti-tumor efficacy in this PDX line. Although GC113 and GC119 showed similarly low levels of ASCT2, their ability to uptake glutamine was higher than that seen in GC117, which could account for the modest anti-tumor efficacy seen in these PDX lines. GC127 and GC84 showed lower basal levels of glutamine uptake as compared to GC113 and GC119. However they showed the highest expression levels of ASCT2, which could account for the lack of anti-tumor efficacy by KM8094. Taking these results into account, it would appear that ASCT2 expression level and the ability to uptake glutamine are potential predictive biomarkers for determining anti-tumor efficacy by KM8094.

Gene expression and DNA methylation array analyses for predictive biomarker candidates

In this regard, we further explored other predictive biomarker candidates by multi-omics analysis on untreated gastric cancer PDX lines by comparing responder against non-responder PDX lines. In the gene expression array analysis (**Figure 4A**), there were a few promising molecules which could be relevant for determining KM8094 efficacy. For example, trefoil factor 2 (TFF2), whose expression level in responders was far higher than that in non-responders, is dominantly expressed in the stomach [17] and secreted preferentially by gastric mucous neck cells [18, 19]. TFF2 has been reported to promote gastric mucosal healing by inhibiting gastric acid secretion and stimulating mucosal proliferation [20]. In addition, TFF2 was suggested as a potential marker of tumor metastasis and

a negative prognostic factor in gastric cancer [21]. Taken together, the proliferative role of TFF2 in normal mucosal cytoprotection could also be a contributing factor towards pathological tumor development in the stomach. In addition, MUC13 could be another notable predictive biomarker candidate for KM8094 efficacy. MUC13 is one of the mucin family proteins that covers the apical surface of the trachea and gastrointestinal tract. It is frequently overexpressed in intestinal-type gastric cancer, but not expressed in normal gastric mucosa [22]. It is to be noted that ASCT2 gene expression in responders was also remarkably lower than that in non-responders, which is consistent with our earlier hypothesis that ASCT2 expression level can be a potential predictive biomarker for KM8094. In the responder PDX lines, 8 genes were differentially expressed and methylated as compared to non-responders (**Figure 4B**). Notably, Angiogenin, ribonuclease, RNase A family, 5 (ANG), was also shortlisted by gene expression array analysis to be a candidate marker (**Figure 4A**). ANG, known as an angiogenesis factor, promotes the growth of tumor cells and was reported to be more highly expressed in gastric cancer tissues as compared to the surrounding non-tumor gastric mucosa [23].

Metabolomics analysis for predictive biomarker candidates

Metabolomics analysis revealed some differences between responders and non-responders. The parameters, AEC and GEC, representing intracellular energy status were prominently higher in non-responders (**Figure 5A**). Also, as shown in **Figure 5B**, GSH and NADPH, which have reducing ability, were apparently higher in non-responders, suggesting non-responders would be resistant to oxidative stress, which may lead to resistance to KM8094 treatment. In addition, some of the substrates for ASCT2, Gln and Cys were clearly high in GC127 and GC84, respectively, which have been defined as a non-responder (**Figure 5C**). The amino acids described above are part of the glutathione production pathway. High expression of ASCT2 in GC84 and GC127 may contribute to high intracellular concentrations of these amino acids. Taking these metabolomics results into account, it is predicted that KM8094 may be effective for the patients with shortage of intracellular energy and lower oxidative stress resistance.

Conclusion

This report demonstrates the therapeutic potential of our novel monoclonal antibody targeting neutral amino acid transporter ASCT2 and provided some insights into clinical predictive biomarker candidates for anti-tumor efficacy. These data would be useful for further progression of KM8094 into future clinical trials. However, more studies would need to be done in order to further delineate their relationship with our target molecule, ASCT2.

Acknowledgements

The manuscript has been reviewed by and approved by all named authors. All named authors have contributed to the manuscript. Noriyuki Kasai, Kenta Hosomi, Aya Sasakawa, Tze Wei Poh, Bernadette Lynn Chua, Toshihiko Ishii, and Kazuya Yamano are employees of Kyowa Hakko Kirin. This study was funded by Kyowa Hakko Kirin. There are no potential conflicts of interests to disclose relevant to the subject of our manuscript. We thank Drs. M. Koike, K. Nakamura, R. Nakai, S. Soga, N. Shiraishi, H. Ando, and T. Takahashi for excellent support and helpful suggestion.

Disclosure of conflict of interest

None.

Abbreviations

ADCC, Antibody-dependent cellular cytotoxicity; ADP, Adenosine diphosphate; AEC, Adenylate energy charge; AMP, Adenosine monophosphate; ASC, Alanine-serine-cysteine; ASCT2, ASC amino acid transporter 2; ATP, Adenosine triphosphate; BSA, Bovine serum albumin; CE-MS, Capillary electrophoresis-mass spectrometry; DAB, 3,3'-Diaminobenzidine; ERK, Extracellular signal-regulated kinase; FDR, False discovery rate; GDP, Guanosine diphosphate; GEC, Guanylate energy charge; GMP, Guanosine monophosphate; GSH, Glutathione-SH; GTP, Guanosine triphosphate; HE, Haematoxylin and eosin; IHC, Immunohistochemistry; MFI, Mean fluorescent intensity; mTOR, Mammalian target of rapamycin; PBMC, Peripheral blood mononuclear cell; PBS, Phosphate buffered saline;

PDX, Patient-derived xenograft; PFA, Paraformaldehyde; PNS, Phosphate buffered saline; ROS, Reactive oxygen species; SD, Standard deviation; SLC1A5, Solute linked carrier family 1 member A5.

Address correspondence to: Noriyuki Kasai, Singapore Translational Research Laboratory, Kyowa Hakko Kirin (Singapore) Pte. Ltd., 11, Biopolis Way, 138667, #05-08 Helios, Singapore. Tel: +65-6774-4505; Fax: +65-6836-3928; E-mail: noriyuki.kasai@kyowa-kirin.co.jp

References

[1] Brenner H, Rothenbacher D, Arndt V. Epidemiology of stomach cancer. Methods Mol Biol 2009; 472: 467-477.

[2] Hartgrink HH, Jansen EP, van Grieken NC, van de Velde CJ. Gastric cancer. Lancet 2009; 374: 477-490.

[3] Kamangar F, Dores GM, Anderson WF. Patterns of cancer incidence, mortality, and prevalence across five continents: defining priorities to reduce cancer disparities in different geographic regions of the world. J Clin Oncol 2006; 24: 2137-2150.

[4] Witte D, Ali N, Carlson N, Younes M. Overexpression of the neutral amino acid transporter ASCT2 in human colorectal adenocarcinoma. Anticancer Res 2002; 22: 2555-2557.

[5] Fuchs BC, Bode BP. Amino acid transporters ASCT2 and LAT1 in cancer: partners in crime? Semin Cancer Biol 2005; 15: 254-266.

[6] Baggetto LG. Deviant energetic metabolism of glycolytic cancer cells. Biochimie 1992; 74: 959-974.

[7] Mazurek S, Eigenbrodt E. The tumor metabolome. Anticancer Res 2003; 23: 1149-1154.

[8] Fuchs BC, Finger RE, Onan MC, Bode BP. ASCT2 silencing regulates mammalian target-of-rapamycin growth and survival signaling in human hepatoma cells. Am J Physiol Cell Physiol 2007; 293: C55-63.

[9] Nicklin P, Bergman P, Zhang B, Triantafellow E, Wang H, Nyfeler B, Yang H, Hild M, Kung C, Wilson C, Myer VE, MacKeigan JP, Porter JA, Wang YK, Cantley LC, Finan PM, Murphy LO. Bidirectional transport of amino acids regulates mTOR and autophagy. Cell 2009; 136: 521-534.

[10] Hassanein M, Hoeksema MD, Shiota M, Qian J, Harris BK, Chen H, Clark JE, Alborn WE, Eisenberg R, Massion PP. SLC1A5 mediates glutamine transport required for lung cancer cell growth and survival. Clin Cancer Res 2013; 19: 560-570.

[11] Wang Q, Hardie RA, Hoy AJ, van Geldermalsen M, Gao D, Fazli L, Sadowski MC, Balaban S, Schreuder M, Nagarajah R, Wong JJ, Metierre C, Pinello N, Otte NJ, Lehman ML, Gleave M, Nelson CC, Bailey CG, Ritchie W, Rasko JE, Holst J. Targeting ASCT2-mediated glutamine uptake blocks prostate cancer growth and tumour development. J Pathol 2015; 236: 278-289.

[12] Suzuki M, Toki H, Furuya A, Ando H. Establishment of monoclonal antibodies against cell surface domains of ASCT2/SLC1A5 and their inhibition of glutamine-dependent tumor cell growth. Biochem Biophys Res Commun 2017; 482: 651-657.

[13] Jin K, Teng L, Shen Y, He K, Xu Z, Li G. Patient-derived human tumour tissue xenografts in immunodeficient mice: a systematic review. Clin Transl Oncol 2010; 12: 473-480.

[14] Tentler JJ, Tan AC, Weekes CD, Jimeno A, Leong S, Pitts TM, Arcaroli JJ, Messersmith WA, Eckhardt SG. Patient-derived tumour xenografts as models for oncology drug development. Nat Rev Clin Oncol 2012; 9: 338-350.

[15] Malaney P, Nicosia SV, Davé V. One mouse, one patient paradigm: new avatars of personalized cancer therapy. Cancer Lett 2014; 344: 1-12.

[16] Lauren P. The two histological main types of gastric carcinoma: diffuse and so-called intestinal-type carcinoma. Acta Pathol Microbiol Scand 1965; 64: 31-49.

[17] Tomasetto C, Rio MC, Gautier C, Wolf C, Hareuveni M, Chambon P, Lathe R. hSP, the domain-duplicated homolog of pS2 protein, is co-expressed with pS2 in stomach but not in breast carcinoma. EMBO J 1990; 9: 407-414.

[18] Lefebvre O, Wolf C, Kédinger M, Chenard MP, Tomasetto C, Chambon P, Rio MC. The mouse one P-domain (pS2) and two P-domain (mSP) genes exhibit distinct patterns of expression. J Cell Biol 1993; 122: 191-198

[19] Jeffrey GP, Oates PS, Wang TC, Babyatsky MW, Brand SJ. Spasmolytic polypeptide: a trefoil peptide secreted by rat gastric mucous cells. Gastroenterology 1994; 106: 336-345.

[20] Farrell JJ, Taupin D, Koh TJ, Chen D, Zhao CM, Podolsky DK, Wang TC. TFF2/SP-deficient mice show decreased gastric proliferation, increased acid secretion, and increased susceptibility to NSAID injury. J Clin Invest 2002; 109: 193-204.

[21] Dhar DK, Wang TC, Maruyama R, Udagawa J, Kubota H, Fuji T, Tachibana M, Ono T, Otani H, Nagasue N. Expression of cytoplasmic TFF2 is a marker of tumor metastasis and negative prognostic factor in gastric cancer. Lab Invest 2003; 83: 1343-1352.

[22] Shimamura T, Ito H, Shibahara J, Watanabe A, Hippo Y, Taniguchi H, Chen Y, Kashima T, Ohtomo T, Tanioka F, Iwanari H, Kodama T, Kazui T, Sugimura H, Fukayama M, Aburatani H. Overexpression of MUC13 is associated with intestinal-type gastric cancer. Cancer Sci 2005; 96: 265-273.

[23] Chen Y, Zhang S, Chen YP, Lin JY. Increased expression of angiogenin in gastric carcinoma in correlation with tumor angiogenesis and proliferation. World J Gastroenterol 2006; 12: 5135-5139.

Supplementary Table 1. Clinical data of patients used for establishment of gastric cancer patient-derived xenograft mouse models

PDX line	Gross description of tumor	Microscopic description
GC119 (Female, 81 years old, Chinese)	Location: Along lesser curve and involving posterior antrum and focally extending to anterior antrum Perforation: No Size (maximum diameter): 9.0 × 8.5 cm Depth of invasion: Muscularis propria Other Pathology: ● Chronic gastritis with antral intestinal metaplasia ● High grade dysplasia is present at the edge of the tumor ● Lymph node metastasis are present (20/31)	Histological tumor type: Adenocarcinoma Histological pattern: - WHO classification: Mixed mucinous (approximately 50%), tubular and papillary adenocarcinoma with focal solid areas. - Lauren Classification: Intestinal type Histological grade: Moderately differentiated (There are areas ranging from well to moderately differentiated, with focal more solid, cribriformed areas suggestive of higher grade.) pT3
GC117 (Female, 73 years old, Chinese, TS1 treated)	Location: Antrum Perforation: No Size: 5.5 × 3.0 × 1.0 cm Depth of invasion: Subserosa Other Pathology: ● Tumor invades subserosa, pT3 ● 3 out of 41 lymph nodes positive for metastatic carcinoma (pN2)	Histological tumor type: Adenocarcinoma, Histological pattern: - WHO classification: Tubular - Lauren classification: Intestinal Histological grade: (Only for WHO tubular carcinoma): Poorly differentiated (5-49% gland formation)
GC127 (Male, 78 years old, other race)	Location: gastro-oesophageal junction Perforation: No Size: 3.5 × 3.0 cm Depth of invasion: Muscularis propria Other Pathology: ● Twelve lymph nodes with no evidence of metastatic carcinoma (0/12)	Histological tumor type: Adenocarcinoma. Histological pattern: - WHO classification: tubular carcinoma - Lauren classification: Intestinal. Histological grade: Moderately to poorly differentiated
GC84 (Male, 93 years old, Chinese)	Location: Incisura Perforation: No Size: 6.0 × 5.5 × 1.2 cm (depth) Depth of invasion: Beyond muscularis mucosa and less than 0.1 cm from serosa Other Pathology: ● Background of H. pylori-associated chronic active gastritis with intestinal metaplasia ● Omentum negative for carcinoma ● 21 lymph nodes without metastatic carcinoma (0/21)	Histological tumor type: Adenocarcinoma Histological pattern: - WHO classification: Tubular/solid type - Lauren classification: Intestinal type Histological grade: Poorly differentiated
GC113 (Female, 77 years old, Chinese)	Location: Posterior wall of the antrum Perforation: No Size: 4.5 × 3.0 × 1.0 cm Depth of invasion: Submucosa Other Pathology: ● Lymphovascular invasion is present ● Lymph nodes negative for metastatic carcinoma (0/40), pNO	Histological tumor type: Adenocarcinoma Histological pattern: - WHO classification: Tubular - Lauren classification: Intestinal type Histological grade: Moderately differentiated